

## Visual object detection biases escape trajectories following acoustic startle in larval zebrafish

### Highlights

- Larval zebrafish use visual scene information to avoid collisions with obstacles
- Barrier avoidance rate corresponds to the absolute distance of obstacles
- The computation of barrier avoidance is covert
- Excitatory bias to the Mauthner cell ipsilateral to approached barriers biases escape

### Authors

Hanna Zwaka, Olivia J. McGinnis, Paula Pflitsch, Srishti Prabha, Vikash Mansinghka, Florian Engert, Andrew D. Bolton

### Correspondence

andrewdbolton@gmail.com

### In brief

Zwaka et al. find that zebrafish robustly bias escape swims away from barriers to avoid collisions. They show that barrier avoidance corresponds to the absolute distance of obstacles and that the computation of barrier avoidance is covert. Finally, they pinpoint components of the circuit responsible for the bias using two-photon laser ablations.

Article

# Visual object detection biases escape trajectories following acoustic startle in larval zebrafish

Hanna Zwaka,<sup>1,3</sup> Olivia J. McGinnis,<sup>1,3</sup> Paula Pflitsch,<sup>1</sup> Srishti Prabha,<sup>1</sup> Vikash Mansinghka,<sup>2</sup> Florian Engert,<sup>1</sup> and Andrew D. Bolton<sup>1,2,4,\*</sup>

<sup>1</sup>Department of Molecular and Cellular Biology, Harvard University, Cambridge, MA 02138, USA

<sup>2</sup>Department of Brain and Cognitive Sciences, MIT, Cambridge, MA 02142, USA

<sup>3</sup>These authors contributed equally

<sup>4</sup>Lead contact

\*Correspondence: [andrewdbolton@gmail.com](mailto:andrewdbolton@gmail.com)

<https://doi.org/10.1016/j.cub.2022.10.050>

## SUMMARY

In this study, we investigated whether the larval zebrafish is sensitive to the presence of obstacles in its environment. Zebrafish execute fast escape swims when in danger of predation. We posited that collisions with solid objects during escape would be maladaptive to the fish, and therefore, the direction of escape swims should be informed by the locations of barriers. To test this idea, we developed a closed-loop imaging rig outfitted with barriers of various qualities. We show that when larval zebrafish escape in response to a non-directional vibrational stimulus, they use visual scene information to avoid collisions with obstacles. Our study demonstrates that barrier avoidance rate corresponds to the absolute distance of obstacles, as distant barriers outside of collision range elicit less bias than nearby collidable barriers that occupy the same amount of visual field. The computation of barrier avoidance is covert: the fact that fish will avoid barriers during escape cannot be predicted by its routine swimming behavior in the barrier arena. Finally, two-photon laser ablation experiments suggest that excitatory bias is provided to the Mauthner cell ipsilateral to approached barriers, either via direct excitation or a multi-step modulation process. We ultimately propose that zebrafish detect collidable objects via an integrative visual computation that is more complex than retinal occupancy alone, laying a groundwork for understanding how cognitive physical models observed in humans are implemented in an archetypal vertebrate brain.

## INTRODUCTION

The ability of humans and animals to interact with objects in the environment is mediated by our understanding of how the physical world works (i.e., “intuitive physics”<sup>1,2</sup>). One perspective on how animal brains enact behavior assumes that interactions with objects are encoded in a “reactive policy”: a mapping between patterns of neural activity on the sensors (e.g., the retina) and corresponding adaptive behaviors. This account is consistent with the widespread view that animals are best understood as input-output machines<sup>3,4</sup> that flourish within a limited environment. The nematode *C. elegans*, for example, directly transforms sensed photic, touch, and chemical stimuli into stereotyped approach and avoidance behaviors.<sup>5–7</sup> These sensory inputs can be modulated by circuitry encoding the physiological state of the animal or the acquired valence of the stimulus; however, the integration of signals from multiple sensors into a unified “world” reflecting the rich features of the external environment has not been shown in the worm. If zebrafish perceived objects only implicitly, via a reactive policy, we would predict that specific light patterns on the 2D retina would map to a fixed set of state-dependent behaviors that are adaptive within its environment. Previous research has suggested that this may be the case (e.g., the optomotor and optokinetic responses,

phototaxis, and visual and acoustic startle; see Portugues and Engert<sup>8</sup> for review). Indeed, some studies have proposed that the proportion of active neurons on the 2D retinal grid (aka retinal or visual occupation) is a means for detecting prey versus predators.<sup>9,10</sup>

An alternative theory is that more advanced animals possess a three-dimensional model of objects in the external world that is referenced when integrating multi-sensory information. Sensors in more complex animals and humans appear to converge on a unified representation of physical space: objects detected by vision, for example, are expected to feel like something, and auditory spatial cues often predict that a visual stimulus will appear.<sup>11</sup> By persistently tracking the state of objects such as obstacles and prey, this kind of model supports “covert” computations that do not require immediate motor responses, instead allowing dynamic multi-sensory scenes to inform future behavioral choices.<sup>1,12,13</sup> In animals like frogs or owls, this manifests as covert tracking of sounds or vibrations so that the animal is able to strike more quickly when the visual appearance of a prey occurs.<sup>14,15</sup> In a human example, if a child is walking on a sidewalk, their parent might notice that they are not paying attention to the road. This would not result in immediate overt behavior of the parent, but the sound of an approaching car would induce a protective reaction that would not have occurred

without the parent's covert computation of their child's wandering state.

It remains an open question at what point in evolution the transition from reactive behavior via independent senses to more integrative object representation began to occur. Earlier studies have suggested that simple animals like chicks and frogs possess some aspects of physical cognition when interacting with objects.<sup>16–18</sup> This paper studies the question of whether an even more neurally accessible organism, the larval zebrafish, possess the ability to bias behavior based on detected objects. Specifically, we wondered if zebrafish visually compute the locations of obstacles in their escape path “just in case” a predator attack induces the fish to flee. Previous studies have shown that when zebrafish escape from predators or experimental stimuli (e.g., air puffs, tank taps, and looming stimuli), their brainstem escape network (BEN) mediates a two alternative behavioral choice<sup>19–24</sup>: fish direct a fast ballistic escape swim (10 ms latency) to either the left or the right. Conduction delays of vision (60 ms in zebrafish) are far slower than the time between stimulus onset and the escape response, meaning that to avoid collisions during escape, fish must use pre-computed visual statistics to generate a bias to their escape trajectories.<sup>25</sup>

Here, we show that startled zebrafish reliably avoid collisions by directing their escapes away from barriers located in their escape path. If the barrier is on the left, they escape right and vice versa. We confirm that visual signals are necessary for the induction of the bias, since fish execute unbiased escapes and collide randomly with barriers in the dark. Keeping the retinal occupancy steady but varying physical size and distance of barriers, we demonstrate that fish are sensitive to the absolute distance of barriers and use a more complex mechanism to measure distance than visual occupancy alone. In light of this result, we propose plausible behavioral algorithms by which fish could detect distance.<sup>26,27</sup> Furthermore, we determine that escape bias is a covert computation that cannot be gleaned from observing routine swimming among barriers. We ultimately suggest a circuit motif whereby visual information either directly or indirectly induces an increase in the excitability of the Mauthner neuron responsible for escapes away from barriers. In summary, the use of one modality (vision) to impact the response of another modality (somatosensory/auditory), the sensitivity of the behavior to absolute barrier distance, and the covert nature of barrier avoidance combine to suggest a more complex representation of physical space in the zebrafish than previously appreciated.

## RESULTS

### Barrier avoidance during escape

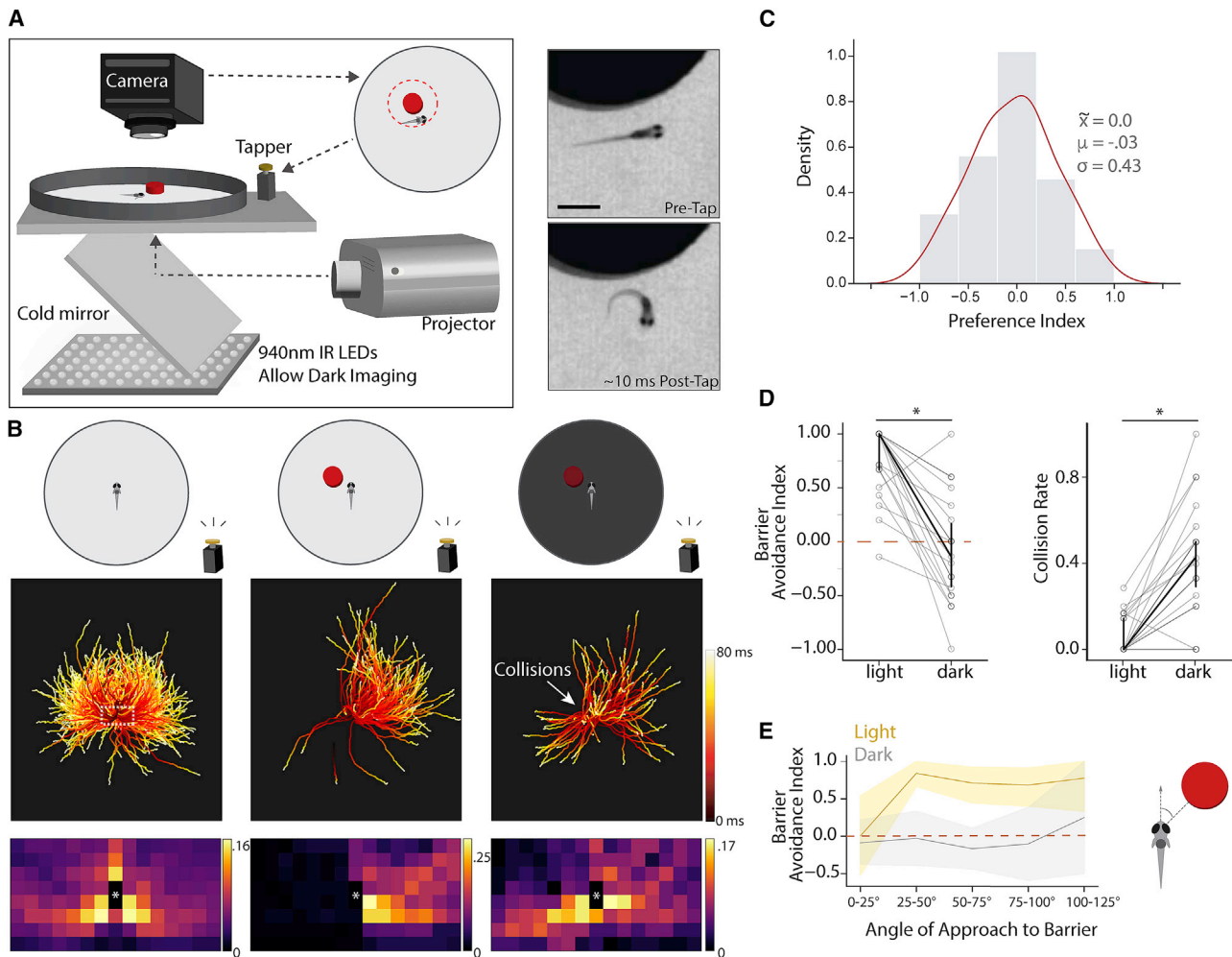
To characterize larval zebrafish escape trajectories in response to a non-directional startle stimulus, fish were imaged at high speed (500 Hz) while swimming in a 12 cm diameter tank (Figure 1A). Custom computer vision software was designed to detect fish entry into a 12 mm wide circular zone located 4 cm from the tank edge. The location of the zone was unmarked and unknown to the fish. Upon zone entry, the detection software triggers a “tap” via an electromagnet that strikes the tank with a metal rod for 200 ms. This stimulus reliably evoked fast escapes at extremely short latency<sup>23</sup> (Figure 1A, right panel;

Figure S1). 98 zebrafish were subjected to this assay in the absence of barriers. The direction of escape in this control condition was random (Figures 1B and 1C). We introduce two indices that describe the direction of escapes in our assay. First, preference index (PI) is  $(\# \text{rightward escapes} - \# \text{leftward escapes}) / (\# \text{total escapes})$ . Calculating this metric for each fish in the absence of barriers yielded a median ( $\bar{x}$ ) PI of 0.0 and mean ( $\mu$ ) of  $-0.03$ , indicating no average preference for one direction or the other ( $p = 0.468$ , Wilcoxon signed-rank; Figure 1C). Individual fish are most commonly unbiased in their escape which is indicated by the highest density of the normal PI distribution centered around the 0.0 bin (Figure 1C). Figure 1B (left panel) shows the time course of escape trajectories following stimulus delivery, and the 2D histogram below illustrates the unbiased distribution of locations visited by the fish immediately after the tap.

Zebrafish tested in control conditions were also subjected to an additional set of trials assessing the same behavior in the presence of barriers, with each fish tested on one of an array of barrier conditions. To characterize barrier avoidance, we introduce a second statistic, barrier avoidance index (BAI), which is  $(\# \text{escapes away from barrier} - \# \text{escapes toward barrier}) / (\# \text{total escapes})$ . For our initial barrier condition, we placed a 12 mm wide, 6 mm high red acrylic barriers into the tank at the same relative tap zone described above, triggering taps when fish passed within 2 mm of the barrier. The introduction of a barrier completely changed the distribution of escape directions. Fish significantly directed their escape trajectories away from the barrier (Figure 1B, center panel; BAI  $\mu = 0.78$ ,  $\bar{x} = 1.0$ ,  $p = 9.5e-7$ ). This bias away from barriers, however, disappeared if the same fish were tested in the dark (Figure 1B, right panel), which is also shown by pairwise comparisons of BAI for fish tested in both light and dark conditions in Figure 1D (dark BAI  $\mu = -0.07$ ,  $\bar{x} = -0.14$ ;  $p = 4.77e-5$ , Wilcoxon signed-rank versus light). Moreover, lack of barrier avoidance in the dark leads to a significant increase in collision rate (Figure 1D right panel;  $\bar{x}$  collision rate: light, 0.0; dark, 0.43;  $p = 2.3e-4$ ). We therefore conclude that zebrafish use vision to detect barriers and reliably avoid collisions by converting their typically random escape directions into laterally biased trajectories.

One phenomenon observed during barrier trials that points to the fish's behavioral algorithm is that barrier avoidance depends on the angle of barrier approach. In the dark, escapes were unbiased, regardless of the angle of approach (Figure 1E). However, in light conditions, if fish approach barriers “head-on” ( $0^\circ$ – $25^\circ$  on either side), their escape trajectories are unbiased and resemble trajectories in dark conditions (bootstrap 95% confidence interval contains 0.0 BAI; yellow line Figure 1E). In this study, we therefore exclude head-on barrier approaches ( $-25^\circ$  to  $25^\circ$  angle of approach) when making comparisons between barrier conditions.

In order to investigate which features of barriers trigger avoidance, we performed the tap assay while varying the height, width, distance, and color of the barrier. BAI under all tested conditions is plotted in descending order of effect in Figure 2. Doubling the distance (4 mm) to the same sized barrier as in Figure 1 continued to bias escapes away from barriers (BAI  $\mu = 0.27$ ,  $\bar{x} = 0.25$ ,  $p = 0.007$ , Wilcoxon signed-rank), but the effect was significantly reduced relative to the 2 mm distance shown in Figure 1 ( $p = 0.00016$ , Mann-Whitney U on BAI at 2 versus 4 mm



**Figure 1. Zebrafish switch from randomly directed to biased escapes upon visual detection of barriers**

(A) Left: overview of experimental setup. Right: typical large-angle short-latency escape turn after tap delivery.

(B) Escape trajectories after tap induction, color coded to reflect time, are shown for 3 conditions (no barriers in visible light, barrier in the visible light, barrier in the dark). Trajectories begin 20 ms after tap command and trajectories with barrier approaches to the right are reflected across the y axis. 2D histograms depict probability of the escape trajectory passing through a spatial bin for each condition. White asterisk indicates starting position of the fish. Barriers are 12 mm wide and 6 mm high, and fish are tapped when they pass within 2 mm of the barrier (N = 98, n = 967; N = 22, n = 128; N = 21, n = 102).

(C) Distribution of preference index for left versus right escapes in no barrier conditions (N = 98).

(D) Pairwise comparison of barrier avoidance index ( $p = 4.77e-5$ ) and collision rate ( $p = 2.3e-4$ ) in fish tested in both the light and dark (same fish as B middle and right panels). Error bars mark 95% CI of the median.

(E) Avoidance index per fish per window of approach angle to the barrier in the light (yellow) and in the dark (light gray). In the light, escapes are not biased in the frontal 25° of visual space but are biased (95% CI above 0) for all other windows. Solid lines represent mean and shaded areas 95% CI. Scale bars in trajectory plots = 2.5 mm; scale bars in 2D histograms = 1.25 mm. Area in dotted box in left (B) panel reflects area plotted in 2D histograms. See Figure S1 for latency and turn amplitude statistics and Figure S2, which shows that naturally biased fish in control barrier-free conditions invert their preference when a barrier is on the side of their bias. See also Figures S1 and S2.

distance). This reduction in barrier avoidance scaled with the predicted probability of colliding with the barrier at these two distances (44% collision rate at 2 mm to 20% at 4 mm,  $p = 1.08e-8$ , Mann-Whitney U, Figure 2A, top, and Figure 2 legend), consistent with the hypothesis that zebrafish map barrier locations to avoid collisions.

We next wondered whether the decreased apparent width and height of the barrier due to increased distance was responsible for the observed reduction in avoidance. Doubling the height of the 4 mm distant barrier (12 mm high) did not significantly change

barrier avoidance (BAI  $\mu = 0.36$ ,  $\bar{x} = 0.20$ ;  $p = 0.25$ , Mann-Whitney U). However, doubling the width (24 mm wide, 6 mm high) significantly increased barrier avoidance ( $\mu = 0.67$ ,  $\bar{x} = 0.78$ ;  $p = 0.0010$ , Mann-Whitney U, 24 versus 12 mm width), initially suggesting that the amount of horizontal retinal occupancy may be a key factor in determining bias. We tested this idea by placing a barrier that occupied the exact same amount of the horizontal and vertical visual field as the 24 mm wide barrier but instead at 8 mm away, reducing the probability of collision to near 0 (Figure 2, top panel). Interestingly, vertical and horizontal visual field

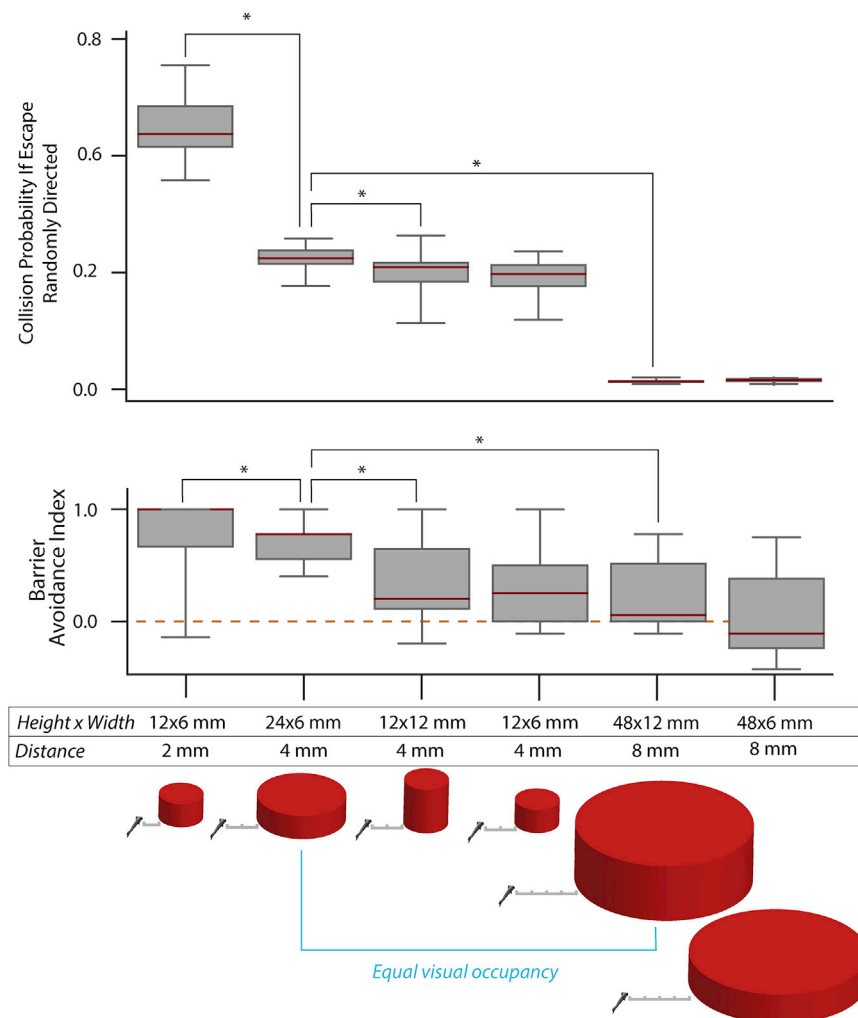


**Figure 2. Barrier avoidance depends on barrier size and distance**

Collision probability is calculated as follows: for each trial within a barrier condition, the heading angle of the fish and the angle to the barrier immediately preceding escape are stored. Each of the 967 trajectories in Figure 1B (no barrier), which reflect the escape behavior of unbiased fish, are then simulated from the stored starting conditions. Intersections between simulated control trajectories and barriers are recorded and divided by the total # of control trajectories to obtain a collision probability per trial. Collision probability therefore reflects how often an unbiased fish would collide with the barriers that subjects encountered during the different barrier conditions. Barrier avoidance decreases in concert with collision probability. The avoidance is also significantly different for barriers with the same retinal occupancy but different distance (blue line) ( $N = 22, 17, 16, 13, 12, 7$ ;  $n = 128, 150, 148, 122, 104, 56$ ). Scale bar ticks in diagram, 2 mm. See Figure S3 for a comparison of angle of approach in the shared visual occupancy conditions that suggests a very similar visual input. Mann-Whitney U results: collisions, conditions 1 and 2,  $p = 2.5e-7$ ; conditions 2 and 3,  $p = 0.014$ ; conditions 2–5,  $p = 8.7e-6$ ; BAI, conditions 1 and 2,  $p = 0.047$ ; conditions 2 and 3,  $p = 0.009$ ; conditions 2–5,  $p = 8.1e-4$ . In boxplots, medians are indicated in red and boxes indicate the interquartile range.

See also Figure S3.

experimentally by projecting stimuli onto the floor of the tank to create differential motion or brightness levels to the left versus right side of the fish.<sup>29</sup> We decided to test whether the same neural circuit elements that govern the laterality of

occupancy was not the most important factor in biasing escapes. Although apparent size is identical between the two conditions (24 mm w, 6 mm h, 4 mm d versus 48 mm w, 12 mm h, and 8 mm d), distance was the determining factor in biasing escapes, as median BAI dropped from 0.78 at 4 mm distance to 0.06 at 8 mm distance ( $p = 0.0008$ , Mann-Whitney U 4 versus 8 mm). Predicted collision statistics in Figure 2 show that the probability of colliding in these two conditions significantly drops from 22% to 1% ( $p = 8.7e-6$ , Mann-Whitney U on predicted collision rates); this suggests that the zebrafish's escape strategy accounts for not only how far away barriers are in their environment but also how far their escape trajectories propel them in space.

### Barrier collidability is a covert computation

Larval zebrafish swim in discrete "bouts" that occur approximately every second. In the absence of attractive or aversive stimuli (aka "routine swimming"), the direction of swim bouts proceeds via stochastic alternating turn chains that equally balance left and right turns.<sup>28</sup> Routine swimming, however, can be biased to the left or right by global motion (optomotor response) or luminance cues (phototaxis) in the environment.<sup>8,29</sup> In fact, skewed turning angle distributions are easily evoked

routine swimming also participate in biasing escapes away from barriers. We reasoned that if zebrafish avoid obstacles during routine navigation, the computation of barrier avoidance during escape should be considered "overt." In other words, the experimenter can tell from overt evidence during routine swimming that the fish will avoid barriers during escape. One could then conclude that the circuitry for routine swimming bias and escape bias may overlap. On the other hand, if the direction of routine swimming and escape were unrelated, the decision to avoid a nearby barrier during escape could be considered covert, meaning the experimenter cannot tell that a fish was planning to escape away from a barrier simply by observing its routine swimming behavior. Similar covert phenomenon have been observed in other animals, where, for example, the spatial location of an animal's gaze is not always correlated to the locus of spatial attention (i.e., an observer cannot tell by gaze where the animal is attending in space).<sup>12,13</sup>

Twelve fish were allowed to freely swim in the tank with four 12 mm wide barriers placed according to Figure 3A. We find that fish generally avoid the locations of red barriers during routine swimming. In Figure 3A (left), the complete trajectory of a free swimming fish is displayed. Figure 3B (left) displays

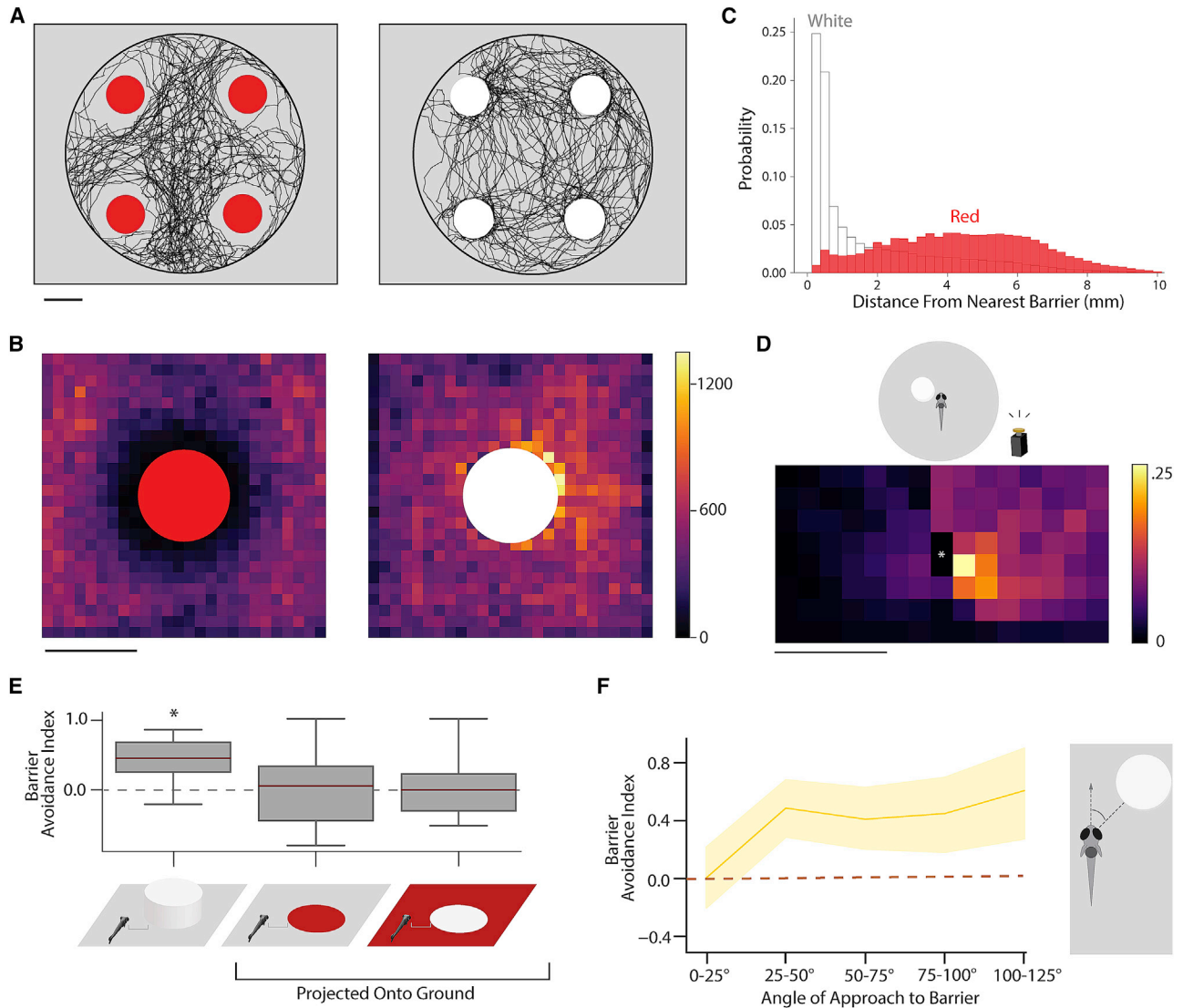


**Figure 3. Red barriers are aversive and white barriers attractive, but both are avoided during escape**

(A) Example trajectories of a zebrafish freely swimming in the arena with four red barriers (left) or four white barriers (right;  $N = 6$ , 6).

(B) Total visits to each spatial bin surrounding red and white barriers.

(C) Distribution of distances from the nearest barrier edge for fish routinely swimming among white and red barriers. Bin size is normalized to the area occupied by each distance. These are the same data that were used to generate the 2D histograms in (B) except a vector is calculated from each coordinate the fish occupies to the nearest barrier edge. Fish coordinates (pooled) are significantly closer to white barriers versus red barriers during routine swimming ( $p < 2.2e-308$ , Mann-Whitney U on coordinate magnitudes). The most common distance fish occupy in white conditions is 0.25 mm from barriers, whereas red is 6.34 mm (modes).

(D) 2D histogram depicting probability of the escape trajectory passing through a spatial bin for white barrier conditions. White asterisk indicates starting position of the fish ( $N = 19$ ,  $n = 254$ ).

(E) Average barrier avoidance index for white physical barriers ( $p = 2.67e-5$ ) and barriers projected onto the floor ( $N = 19, 20, 20$ ;  $n = 254, 160, 146$ ). Medians are indicated in red and boxes indicate the interquartile range.

(F) Barrier avoidance index for different angles of approach to the white barrier in the light (yellow). As with red barriers, escapes are not biased in the frontal 25° of visual space. Solid lines represent mean and shaded areas 95% CI via bootstrap.

Scale bars, 12 mm (A and B) and 1.25 mm (D).

a density plot with the number of visits to each bin of space across all fish. The vicinity surrounding red barriers is the least visited region of the tank, suggesting that fish treat red barriers as aversive. This result suggested initially that there may be overlap between circuits that bias turn direction during routine swimming and escapes; however, we wondered

if we could find a barrier condition that could dissociate avoidance during escapes from overt aversion during free swimming.

We found that replacing red barriers with white barriers of the exact same size completely inverted preference during routine swimming (Figures 3A–3C; see Figure 3 legend). Instead of

avoiding barriers, the zebrafish's routine swimming trajectories reflect an inherent attraction to white barrier locations, and spatial bins bordering the white barrier were the most frequently visited (Figures 3A–3C). Overt evidence from routine swimming, and hypothetical overlap of routine turning and escape bias circuits, would have predicted that fish would also turn toward the white barriers during escape. Remarkably, however, this was not the case. Zebrafish treated white barriers as collidable objects during escapes, significantly biasing their escape turns away from white barriers (Figures 3D and 3E; BAI  $\mu = 0.43$ ,  $\bar{x} = 0.44$ ,  $p = 2.67e-5$ , one-sample Wilcoxon signed-rank). This suggests that the bias circuits are in fact separate and that the tendency of the fish to escape away from barriers is a covert computation that the experimenter cannot observe until evoking an escape. Like red barriers, escapes away from white barriers are not biased in the frontal 25° of visual space, and spatial bins on the side opposite the barrier are the most commonly visited during escapes (Figures 3D and 3F), suggesting the same bias mechanism.

As noted above, bias of turn direction during routine swimming can be instantiated by projecting differential luminance to the left and right sides of the fish.<sup>29</sup> As a further control showing that phototactic-induced bias of routine swimming and escape bias circuits are in fact separate, red circles with the same diameter as a solid barrier were projected onto a gray background and white barriers were projected onto a red background. If luminance cues were responsible for biasing escapes, we would have expected that these stimuli would also bias escape direction. However, zebrafish did not bias their escapes if tapped within 2 mm of a red dot nor a white dot projected onto the bottom of the tank (Figure 3E, right side; BAI  $\mu = 0.028$ ,  $0.037$ ,  $\bar{x} = 0.06$ ,  $0$ ;  $p = 0.86$ ,  $0.98$ ; dots are equal width of barriers). This suggests that color and luminance comparison between the left and right hemifield does not itself play a role in escape and also that barriers must have height to be considered an obstacle.

In sum, the zebrafish does not overtly show in its routine swimming during the white barrier assay that it will escape away from the barrier. Moreover, laterally differential luminance on the bottom of the tank, which induces bias in routine swimming, does not affect the direction of escapes to tap stimuli.

### Mauthner cell ablations reveal candidate biasing circuit motifs

We next performed an initial circuit analysis to determine how the visual system influences the Brainstem Escape Network (BEN). This network mediates two-alternative behavioral choice during escapes and contains the commonly known Mauthner neurons.<sup>19</sup> Mauthner cells, along with their homologs MiD2cm and MiD3cm, play a prominent role in evoking short latency, high amplitude escape turns in fish.<sup>20</sup> Spiking in the right Mauthner neuron is typically correlated with escapes to the left, while left Mauthner spiking coincides with escapes to the right (96%<sup>30</sup>). However, Mauthner cells can co-activate, homologs can also control escape features even in the absence of Mauthner cell activity, and single Mauthner destruction does not always induce unilateral escapes due to homolog contributions.<sup>22,23,31–33</sup> Nonetheless, there is general agreement that the Mauthner neuron plays an essential role in determining the left-right alternative choice for fast escapes when both Mauthner cells are

intact. Since the two-alternative escape choice is strongly influenced by barriers, we wondered how visual information about barrier location impinges upon this complex bilateral circuit. Critically, Mauthner cells receive modulatory inputs from throughout the brain that are conspicuously positioned for biasing escape direction. Since 97% of the taps evoked in our barrier dataset (Figures 1 and 2) resulted in rapid, large amplitude escape turns typically attributed to the BEN (mean 104.4° cumulative tail angle at 11.06 ms post-tap; Figure S1; STAR Methods), we surmised that barrier avoidance could possibly be accomplished via lateralized Mauthner modulation.

There are multiple ways for visual information to influence the Mauthner cells because it receives glutamatergic, GABAergic, glycinergic, and neuromodulatory inputs (Figure 4E).<sup>34</sup> Via primary or neuromodulatory transmitters, visual activity could either inhibit or remove excitation from the Mauthner neuron that pulls the fish toward the barrier or excite/disinhibit the neuron that propels the fish away from the barrier. To uncover whether either of these motifs exist in the zebrafish brain, we fluorescently labeled Mauthner neurons using a custom Gal4 line (Tg(pMH93-16946)<sup>a378</sup>) and ablated a single Mauthner neuron per fish with a two-photon laser (STAR Methods; Figure 4A). As noted, escape direction is typically contralateral to the spiking Mauthner neuron; hence, we expected fish with ablations to preferentially escape away from the side of the intact neuron. In Figure 4B, PI is calculated as (#turns away from intact Mauthner – #turns toward intact Mauthner/#total escape turns). As expected, fish significantly biased their escapes away from the intact Mauthner side when tapped in the absence of barriers (PI away from intact Mauthner  $\bar{x} = 0.53$ ;  $p = 0.0011$ , one-sample Wilcoxon signed-rank; see escapes in barrier-less conditions, Figure 4C). This level of bias is in alignment with previous Mauthner ablation experiments.<sup>23</sup> Critically, when barriers were added to the tank, taps executed when fish approached barriers opposite to the intact Mauthner cell continued to induce escape away from the intact neuron (and resultingly, toward barriers) similar to barrier-less conditions (Figures 4B and 4C), showing a complete loss in the ability to bias escapes away from barriers (PI away from intact Mauthner  $\bar{x} = 0.60$ ,  $p = 0.77$ , paired Wilcoxon-signed rank versus no barrier; Figure 4B). On the other hand, if fish approached barriers on the side of the intact Mauthner cell, their preference for escaping away from the intact neuron was actually significantly facilitated (PI away from intact Mauthner  $\bar{x} = 0.83$ ,  $p = 0.01988$ , paired Wilcoxon signed-rank versus no barrier; Figure 4B). BAI and collision statistics are significantly different for the two conditions (Figure 4D and Figure 4 legend); strikingly, nearly all of the interquartile range of collisions when the barrier is opposite to the intact Mauthner is above 50% collisions per fish, suggesting the complete inability to avoid crashing into obstacles (Figure 4D, upper panel left). Coupled together, these results favor the excitatory/disinhibitory circuit architecture proposed in Figure 4E. To reiterate, the intact Mauthner neuron does not appear to be inhibited by the perception of a contralateral barrier (Figures 4D and 4E), shown by the continued escape toward barriers opposite the intact Mauthner and resultant high collision rate. The Mauthner neuron ipsilateral to a barrier therefore likely undergoes an excitatory or disinhibitory effect during perception of a barrier, enhancing bias up to the levels observed in Figure 2 in the strongest biasing conditions.

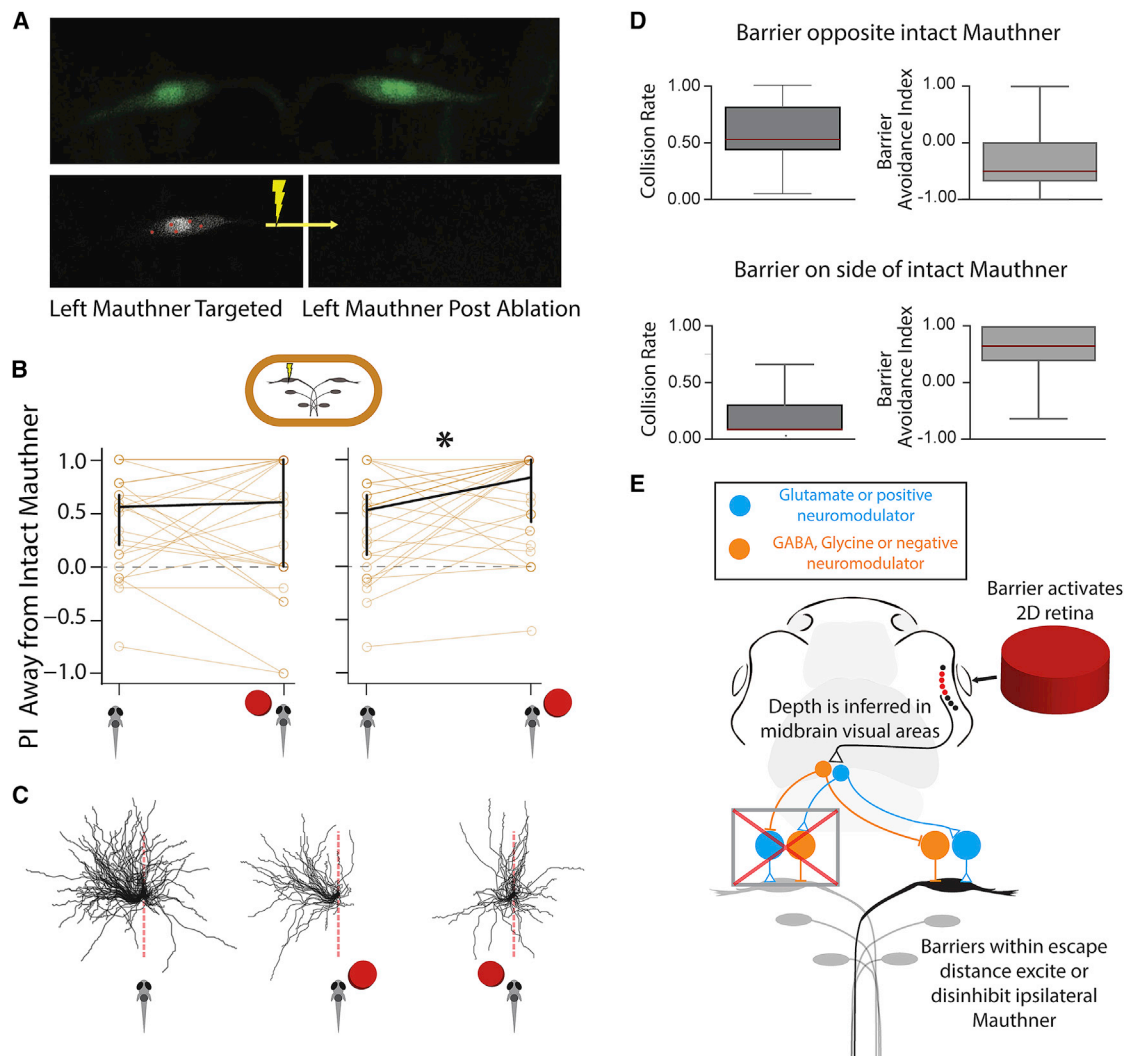


#### Figure 4. Input into ipsilateral Mauthner cell biases escapes

(A) Two-photon image of both Mauthner cells (upper panel) in our custom Gal4 line. Left: Mauthner cell pre-ablation showing our laser targeting protocol for Mauthner destruction. Same cell post ablation.

(B) PI for escapes away from intact Mauthner in control and barrier conditions ( $p = 0.01988$ ) ( $N = 26$ ,  $n = 275$  control, 192 barrier). Error bars are 95% CI of the median.

(C) Individual escape directions for animals with the left Mauthner cell ablated. Fish with an ablated left Mauthner cell show escape bias to the left (left). Escapes in left Mauthner ablated fish with barrier on the right show an increased bias to the left away from the barrier (center), whereas a barrier on the left leads to continued biased escape to the left (toward the barrier). This result suggests that there is no inhibitory mechanism on the intact Mauthner that prevents escapes toward barriers (compare E).

(D) Barrier avoidance index and collision rates for fish with Mauthner cell ablations. Fish no longer avoid barriers if the Mauthner cell on the side of the barrier is ablated; ablations reveal that there is no inhibitory mechanism onto the intact Mauthner that prevents collisions with barriers (i.e., the intact Mauthner continues to pull the fish toward barriers.  $p = 1.6e-5$  and  $2.8e-5$ . Medians are indicated in red and boxes indicate the interquartile range.

(E) Proposed model after integration of Mauthner cell ablation experiments reveals excitatory/disinhibitory input into ipsilateral Mauthner cell, which favors escapes away from barriers. See also [Figure S4](#).

## DISCUSSION

In this study, we investigated object detection by asking whether larval zebrafish are sensitive to the presence of obstacles during fast escape swims. We discovered that when zebrafish are acoustically startled near barriers, they alter their normally unbiased escape direction and instead bias their escapes away from visually detected objects ([Figure 1](#)). We also

show that zebrafish avoid barriers at distances that are within its escape range to avoid collisions ([Figure 2](#)), which resembles the idea of embodied cognition<sup>35,36</sup>; in other words, the fish's visual influence over the escape system is tuned to how far the BEN displaces the body. The remainder of this discussion will delve into the fish's distance sensing capabilities in the context of previous research. The covert nature of escape bias will be further explained and the question of whether the

### Large Barrier Far From Fish

### Small Barrier Close to Fish

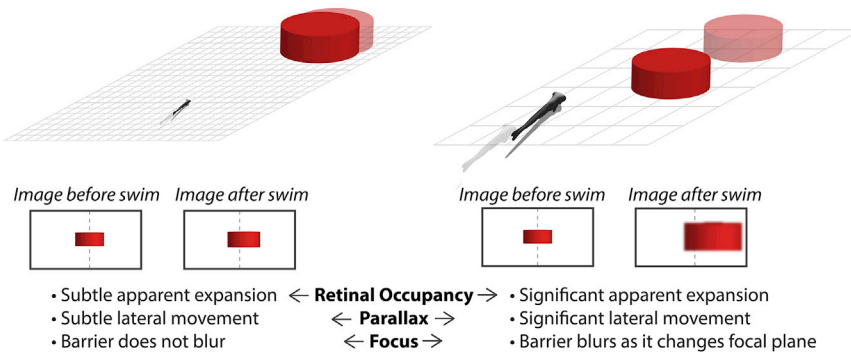


**Figure 5. Three candidate mechanisms for distance computation in our assay**

fish is displaying a primitive model of objects will be addressed. Finally, we propose future experiments that could build upon our neuroscience results and pinpoint neural circuits involved in barrier detection.

As noted in the introduction, cognitive physical models in humans support multimodal integration into a unified representation of the external environment. The transfer of scene information from one modality (vision) into the sensorimotor transformation of another modality (acoustic) in our study appears to be a step toward a more unified representation of the world. Intuitive physical models also allow for covert computations that track object features for future behavioral choices. Our results suggest that fish are performing visual object detection for “just in case situations.” Visual conduction times in the vertebrate retina (60 ms in the zebrafish) are far slower than the latency between tap onset and escape (11 ms in Figure S1).<sup>25</sup> Therefore, for collision avoidance, the mapping of relevant visual features onto the correct neural circuits in the BEN must be pre-computed. We argue in Figure 3 that the state of the escape bias circuit is covert; an observer of routine swimming cannot predict the direction of escape bias. In other words, we cannot tell from the fish’s overt attraction to white barriers that its BEN has been biased away from collisions with the same solid object. Moreover, stimuli known to bias routine swimming (bottom projected differential luminance) were ineffective at biasing escape (Figure 3E). The circuit mediating routine bias and escape bias are therefore separate. It is likely that during routine behavior, the fish computes environmental features that are relevant during unexpected events or emergencies in the world.<sup>37</sup> This appears to be a common feature of physical reasoning in other animals. For example, the location of an adult goldfish within its tank preceding a predator stimulus modifies the fish’s ballistic escape direction; detection of tank walls as impermeable obstacles before escape initiation would be consistent with our findings.<sup>21</sup> Frogs similarly inform their choice of jumping direction according to the location of static objects.<sup>18</sup> Relatedly, the non-cortical brain regions that fish and frogs possess have been shown to play a role in covert computations of object identity in an array of animals.<sup>38,39</sup> In frogs, for example, “attention units” in the optic tectum respond to vibrations of prey-like stimuli that do not immediately prompt hunting behavior. These subthreshold stimuli instead facilitate future prey striking behavior if a prey object is presented in the same location seconds later (i.e., the location

has been stored just in case the vibrating object is a catchable prey). A similar effect has been observed in the barn owl tectum, where multimodal neurons respond to visual cues more strongly if subthreshold auditory cues had previously indicated the location of prey.<sup>15</sup>

Our results show that an important variable influencing escape bias is the absolute distance (“depth”) of the barrier. Sensitivity to distance also appears

in zebrafish prey capture.<sup>36,40</sup> Previous studies have emphasized the role of stimulus “size,” measured by total retinal occupancy, in decoding stimulus identity.<sup>10</sup> However, total retinal occupancy, as shown here, fails to unambiguously convey the distance of a stimulus and, accordingly, its behavioral relevance. Accurate computation of distance is required to estimate the true size of an object and depth must be inferred from the 2D retinal representation—it does not come for “free” with any known visual map (e.g., an equal-sized neural representation on the optic tectum map could be a close prey or a distant barrier). This point is emphasized by previous studies examining the response of zebrafish to live prey and to different-sized moving dots. In prey capture, when a fish strikes at a 300 micron-wide prey item, the prey is so close (avg. 870 + 180 microns) that it occupies 16°–23° of visual space.<sup>36</sup> Moving dots occupying this amount of visual space induce the strongest possible avoidance in previous studies.<sup>9,10</sup> Therefore, our study and previous results suggest that integration of multiple depth cues, including contextual evidence, must be at play. Dynamic lens accommodation and motion cues may play significant roles.<sup>26,41,42</sup> In addition to motion parallax, observed in bees and flies, some insects like locusts and the praying mantis purposefully move their heads from side to side to gain distance information from self-motion.<sup>43–45</sup> In our study, barrier approaches that are head on fail to evoke a bias in our experiments (Figure 1E; –25° to 25° angle of approach); importantly, the window of visual space occupied by the barrier during head-on approach encapsulates the binocular zone,<sup>9</sup> making it unlikely that fish use stereopsis for barrier avoidance. It is helpful to consider the cues that naturally arise for larval zebrafish outside of the binocular zone: during a swim toward a barrier, the barrier will appear to expand, move laterally across the visual scene, and change focal plane, all in proportion to barrier distance when the swim began (Figure 5).

Distance detection appears to be the first step from a 2D-reactive policy to a more structured model of the 3D world. How would future experiments disambiguate whether the zebrafish is executing a complex reactive policy or instead possesses a primitive structured model? One strategy would be to present fish embedded in a virtual reality with controlled visual stimuli that would disambiguate objects to a human or Bayesian observer. For example, if the fish has identified a virtual barrier as large and distant due to parallax, will the fish still approach a stimulus that appears to be a nearby prey (by retinal size,

angular speed) if the prey passes behind the distant barrier? Passing behind the barrier would suggest that the virtual prey is not a nearby prey at all, but a faster moving, larger object that is further away than the barrier. If the fish pursues this stimulus as prey, a more reaction-based, sensorimotor intelligence in the spirit of Brooks and Braitenberg would be assumed.<sup>3,4</sup>

Finally, with respect to neural mechanism, we suggest that the bias we observe is accomplished via an excitatory or disinhibitory effect onto the Mauthner neuron responsible for pulling the fish away from barriers during escape. Ablating one Mauthner neuron did not lead to an abolishment of escapes toward the opposite side of the ablation. This was expected from previous studies on Mauthner ablation<sup>23</sup> and likely emphasizes the capability of Mauthner homologs to compensate for Mauthner neuron loss. Importantly, touch stimulation of the head to induce escapes is the most effective means of recruiting Mauthner homologs and leads to a more vigorous escape.<sup>22</sup> Our non-directional tap stimulus likely induces simultaneous head and tail stimulation, recruiting Mauthner homologs and allowing a bilateral competition between all BEN components across hemispheres. Our final hypothesis suggests either an excitatory or disinhibitory influence to the ipsilateral Mauthner cell that biases escapes away from barriers (Figure 4). In future experiments, we plan on functionally dissecting this input, which we hypothesize may come from the tectum via spiral fiber neurons.<sup>23</sup> Due to the relative simplicity of the tap to Mauthner circuit and the known synaptic connectivity of excitatory, inhibitory, and modulatory inputs to the Mauthner neuron,<sup>34</sup> the zebrafish presents an excellent model for a future circuit characterization. Importantly, the type of elegant circuit analysis performed in previous studies of the zebrafish BEN<sup>19,23</sup> is not yet possible for our behavior of interest using current technologies. This is because we hypothesize that the fish requires motion parallax to estimate barrier distance, which necessitates a comparison between the motion of the barrier and the fish's own motion vector (Figure 5). BEN circuit dissection requires immobile embedded fish, and proper motion parallax delivery requires an immersive visual environment that is tuned to the exact statistics of tail motion. Our group is currently addressing this issue using detailed Bayesian tail models that instantly and accurately update a 3D virtual world. This approach will create accurate motion parallax in an embedded setting, allowing the type of circuit dissection seen in previous studies.

## STAR★METHODS

Detailed methods are provided in the online version of this paper and include the following:

- **KEY RESOURCES TABLE**
- **RESOURCE AVAILABILITY**
  - Lead contact
  - Materials availability
  - Data and code availability
- **EXPERIMENTAL MODEL AND SUBJECT DETAILS**
- **METHOD DETAILS**
  - Behavioral Setup
- **QUANTIFICATION AND STATISTICAL ANALYSIS**
  - Escape Analysis

- Navigation Assay
- Mauthner Neuron Ablations

## SUPPLEMENTAL INFORMATION

Supplemental information can be found online at <https://doi.org/10.1016/j.cub.2022.10.050>.

A video abstract is available at <https://doi.org/10.1016/j.cub.2022.10.050#mmc3>.

## ACKNOWLEDGMENTS

The authors would like to thank Martin Haesemeyer, Josua Jordi, Rob Johnson, Eva Naumann, Tim Dunn, Kirsten Bolton, Kristian Herrera, Clemens Riegler, and Armin Bahl for discussions concerning experimental design and interpretation. Alix Lacoste's excellent thesis defense was especially influential in laying the foundations of this project. All members of the Engert lab were instrumental in weekly discussions. This work was funded by a U19 grant from the NIH.

## AUTHOR CONTRIBUTIONS

A.D.B. designed the study and experimental setup; A.D.B., H.Z., O.J.M., and P.P. carried out the experiments; A.D.B. analyzed the data; A.D.B., H.Z., and O.J.M. interpreted the data; S.P. generated the custom Gal4 line; F.E., H.Z., and V.M. contributed to the analysis of the results; A.D.B., H.Z., and F.E. wrote the manuscript; and A.D.B. and F.E. supervised the project.

## DECLARATION OF INTERESTS

The authors declare no competing interests.

Received: May 11, 2022

Revised: September 27, 2022

Accepted: October 21, 2022

Published: November 18, 2022

## REFERENCES

1. Ullman, T.D., Spelke, E., Battaglia, P., and Tenenbaum, J.B. (2017). Mind games: game engines as an architecture for intuitive physics. *Trends Cogn. Sci.* *21*, 649–665.
2. Battaglia, P.W., Hamrick, J.B., and Tenenbaum, J.B. (2013). Simulation as an engine of physical scene understanding. *Proc. Natl. Acad. Sci. USA* *110*, 18327–18332.
3. Brooks, R.A. (1991). Intelligence without representation. *Artif. Intell.* *47*, 139–159.
4. Braitenberg, V. (1986). *Vehicles: Experiments in Synthetic Psychology* (MIT Press).
5. Bhatla, N., and Horvitz, H.R. (2015). Light and hydrogen peroxide inhibit *C. elegans* feeding through gustatory receptor orthologs and pharyngeal neurons. *Neuron* *85*, 804–818.
6. Chen, X., and Chalfie, M. (2014). Modulation of *C. elegans* touch sensitivity is integrated at multiple levels. *J. Neurosci.* *34*, 6522–6536.
7. Bargmann, C.I., Hartwig, E., and Horvitz, H.R. (1993). Odorant-selective genes and neurons mediate olfaction in *C. elegans*. *Cell* *74*, 515–527.
8. Portugues, R., and Engert, F. (2009). The neural basis of visual behaviors in the larval zebrafish. *Curr. Opin. Neurobiol.* *19*, 644–647.
9. Bianco, I.H., Kampff, A.R., and Engert, F. (2011). Prey capture behavior evoked by simple visual stimuli in larval zebrafish. *Front. Syst. Neurosci.* *5*, 101.
10. Barker, A.J., and Baier, H. (2015). Sensorimotor decision making in the zebrafish tectum. *Curr. Biol.* *25*, 2804–2814.

11. Andersen, R.A. (1997). Multimodal integration for the representation of space in the posterior parietal cortex. *Philos. Trans. R. Soc. Lond. B Biol. Sci.* **352**, 1421–1428.
12. Lovejoy, L.P., and Krauzlis, R.J. (2010). Inactivation of primate superior colliculus impairs covert selection of signals for perceptual judgments. *Nat. Neurosci.* **13**, 261–266.
13. Müller, J.R., Philastides, M.G., and Newsome, W.T. (2005). Microstimulation of the superior colliculus focuses attention without moving the eyes. *Proc. Natl. Acad. Sci. USA* **102**, 524–529.
14. Ingle, D. (1975). Focal attention in the frog: behavioral and physiological correlates. *Science* **188**, 1033–1035.
15. Zahar, Y., Reches, A., and Gutfreund, Y. (2009). Multisensory enhancement in the optic tectum of the barn owl: spike count and spike timing. *J. Neurophysiol.* **101**, 2380–2394.
16. Chiandetti, C., and Vallortigara, G. (2011). Intuitive physical reasoning about occluded objects by inexperienced chicks. *Proc. R. Soc. Lond. B* **278**, 2621–2627.
17. Spelke, E.S., and Lee, S.A. (2012). Core systems of geometry in animal minds. *Philos. Trans. R. Soc. Lond. B Biol. Sci.* **367**, 2784–2793.
18. Ingle, D.J., and Hoff, K.v. (1990). Visually elicited evasive behavior in frogs. *BioScience* **40**, 284–291.
19. Koyama, M., Minale, F., Shum, J., Nishimura, N., Schaffer, C.B., and Fetcho, J.R. (2016). A circuit motif in the zebrafish hindbrain for a two alternative behavioral choice to turn left or right. *eLife* **5**, e16808. <https://doi.org/10.7554/eLife.16808>.
20. Eaton, R.C., Lee, R.K.K., and Foreman, M.B. (2001). The Mauthner cell and other identified neurons of the brainstem escape network of fish. *Prog. Neurobiol.* **63**, 467–485.
21. Eaton, R.C., and Emberley, D.S. (1991). How stimulus direction determines the trajectory of the Mauthner-initiated escape response in a teleost fish. *J. Exp. Biol.* **161**, 469–487. <https://doi.org/10.1242/jeb.161.1.469>.
22. O'Malley, D.M., Kao, Y.H., and Fetcho, J.R. (1996). Imaging the functional organization of zebrafish hindbrain segments during escape behaviors. *Neuron* **17**, 1145–1155.
23. Lacoste, A.B., Schoppik, D., Robson, D., Haesemeyer, M., Portugues, R., Li, J., Randlett, O., Wee, C., Engert, F., and Schier, A. (2015). A convergent and essential interneuron pathway for Mauthner-cell-mediated escapes. *Curr. Biol.* **25**, 1526–1534.
24. Dunn, T.W., Gebhardt, C., Naumann, E.A., Riegler, C., Ahrens, M.B., Engert, F., and Del Bene, F. (2016). Neural circuits underlying visually evoked escapes in larval zebrafish. *Neuron* **89**, 613–628.
25. Van Epps, H.A., Yim, C.M., Hurley, J.B., and Brockerhoff, S.E. (2001). Investigations of photoreceptor synaptic transmission and light adaptation in the zebrafish visual mutant nrc. *Invest. Ophthalmol. Vis. Sci.* **42**, 868–874.
26. Schuster, S., Strauss, R., and Götz, K.G. (2002). Virtual-reality techniques resolve the visual cues used by fruit flies to evaluate object distances. *Curr. Biol.* **12**, 1591–1594.
27. Minsky, M. (2007). *The Emotion Machine: Commonsense Thinking, Artificial Intelligence, and the Future of the Human Mind* (Simon and Schuster).
28. Dunn, T.W., Mu, Y., Narayan, S., Randlett, O., Naumann, E.A., Yang, C.T., Schier, A.F., Freeman, J., Engert, F., and Ahrens, M.B. (2016). Brain-wide mapping of neural activity controlling zebrafish exploratory locomotion. *eLife* **5**, e12741. <https://doi.org/10.7554/eLife.12741>.
29. Huang, K.H., Ahrens, M.B., Dunn, T.W., and Engert, F. (2013). Spinal projection neurons control turning behaviors in zebrafish. *Curr. Biol.* **23**, 1566–1573.
30. Zottoli, S.J. (1977). Correlation of the startle reflex and Mauthner cell auditory responses in unrestrained goldfish. *J. Exp. Biol.* **66**, 243–254. <https://doi.org/10.1242/jeb.66.1.243>.
31. Satou, C., Kimura, Y., Kohashi, T., Horikawa, K., Takeda, H., Oda, Y., and Higashijima, S.i. (2009). Functional role of a specialized class of spinal commissural inhibitory neurons during fast escapes in zebrafish. *J. Neurosci.* **29**, 6780–6793.
32. Liu, K.S., and Fetcho, J.R. (1999). Laser ablations reveal functional relationships of segmental hindbrain neurons in zebrafish. *Neuron* **23**, 325–335.
33. Kohashi, T., and Oda, Y. (2008). Initiation of Mauthner- or non-Mauthner-mediated fast escape evoked by different modes of sensory input. *J. Neurosci.* **28**, 10641–10653.
34. Korn, H., and Faber, D.S. (2005). The Mauthner cell half a century later: a neurobiological model for decision-making? *Neuron* **47**, 13–28.
35. Maturana, H.R., and Varela, F.J. (1987). *The Tree of Knowledge: The Biological Roots of Human Understanding* (New Science Library/Shambhala Publications), p. 263.
36. Bolton, A.D., Haesemeyer, M., Jordi, J., Schaechtle, U., Saad, F.A., Mansinghka, V.K., Tenenbaum, J.B., and Engert, F. (2019). Elements of a stochastic 3D prediction engine in larval zebrafish prey capture. *eLife* **8**, e51975. <https://doi.org/10.7554/eLife.51975>.
37. Dean, P., Redgrave, P., and Westby, G.W.M. (1989). Event or emergency? Two response systems in the mammalian superior colliculus. *Trends Neurosci.* **12**, 137–147.
38. Krauzlis, R.J., Lovejoy, L.P., and Zénon, A. (2013). Superior colliculus and visual spatial attention. *Annu. Rev. Neurosci.* **36**, 165–182. <https://doi.org/10.1146/annurev-neuro-062012-170249>.
39. Lindsay, G.W. (2020). Attention in psychology, neuroscience, and machine learning. *Front. Comput. Neurosci.* **14**, 29.
40. Patterson, B.W., Abraham, A.O., MacIver, M.A., and McLean, D.L. (2013). Visually guided gradation of prey capture movements in larval zebrafish. *J. Exp. Biol.* **216**, 3071–3083.
41. Srinivasan, M.V. (1992). Distance perception in insects. *Curr. Dir. Psychol. Sci.* **1**, 22–26. <https://doi.org/10.1111/1467-8721.ep10767830>.
42. Lock, A., and Collett, T. (1980). The three-dimensional world of a toad. *Proc. R. Soc. Lond. B* **206**, 481–487.
43. Sobel, E.C. (1990). The locust's use of motion parallax to measure distance. *J. Comp. Physiol. A* **167**, 579–588. <https://doi.org/10.1007/BF00192653>.
44. Wallace, G.K. (1959). Visual scanning in the desert locust *Schistocerca gregaria* Forskål. *J. Exp. Biol.* **36**, 512–525. <https://doi.org/10.1242/jeb.36.3.512>.
45. Poteser, M., and Kral, K. (1995). Visual distance discrimination between stationary targets in praying mantis: an index of the use of motion parallax. *J. Exp. Biol.* **198**, 2127–2137.
46. Rauch, G.J., Granato, M., and Haffter, P. (1997). A polymorphic zebrafish line for genetic mapping using SSLPs on high-percentage agarose gels. *Tech. Tips Online* **2**, 148–150. [https://doi.org/10.1016/S1366-2120\(08\)70068-0](https://doi.org/10.1016/S1366-2120(08)70068-0).
47. Scott, E.K., Mason, L., Arrenberg, A.B., Ziv, L., Gosse, N.J., Xiao, T., et al. (2007). Targeting neural circuitry in zebrafish using GAL4 enhancer trapping. *Nat. Methods* **4**, 323–327.
48. Dunn, T.W., and Fitzgerald, J.E. (2020). Correcting for physical distortions in visual stimuli improves reproducibility in zebrafish neuroscience. *eLife* **9**, e53684. <https://doi.org/10.7554/eLife.53684>.
49. Karlsson, J., von Hofsten, J., and Olsson, P.E. (2001). Generating transparent zebrafish: a refined method to improve detection of gene expression during embryonic development. *Mar. Biotechnol. (NY)* **3**, 522–527. <https://doi.org/10.1007/s1012601-0053-4>.
50. Whittaker, J.R. (1966). An analysis of melanogenesis in differentiating pigment cells of ascidian embryos. *Dev. Biol.* **14**, 1–39. [https://doi.org/10.1016/0012-1606\(66\)90003-0](https://doi.org/10.1016/0012-1606(66)90003-0).
51. Tsai, P.S., Blinder, P., Migliori, B.J., Neev, J., Jin, Y., Squier, J.A., and Kleinfeld, D. (2009). Plasma-mediated ablation: an optical tool for submicrometer surgery on neuronal and vascular systems. *Curr. Opin. Biotechnol.* **20**, 90–99.

## STAR★METHODS

### KEY RESOURCES TABLE

REAGENT or RESOURCE	SOURCE	IDENTIFIER
Deposited data		
Raw and analyzed data	This paper	<a href="https://www.dropbox.com/sh/c9dk5scldm73v/AADXoOlwljJEANa1dvdTG9Bla?dl=0">https://www.dropbox.com/sh/c9dk5scldm73v/AADXoOlwljJEANa1dvdTG9Bla?dl=0</a>
Experimental models: Organisms/strains		
Zebrafish: 7-9 days post fertilization; <i>Danio rerio</i> : WIK wildtype	Rauch et al. <sup>46</sup>	ZFIN: ZDB-GENO-010531-2
Zebrafish: 7-9 days post fertilization; <i>Danio rerio</i> : Tg(pMH93-16946) <sup>a378</sup> x Tg(UAS-E1b:Kaede)s1999t	This study, Scott et al. <sup>47</sup>	N/A, ZFIN:ZDB-ALT-070314-1
Software and algorithms		
Python analysis software	This study	<a href="https://github.com/larrylegend33/Escape-Analysis">https://github.com/larrylegend33/Escape-Analysis</a>
C# behavioral setup software	This study	<a href="https://github.com/larrylegend33/EscapeCode">https://github.com/larrylegend33/EscapeCode</a>

### RESOURCE AVAILABILITY

#### Lead contact

Further information and requests for resources should be directed to and will be fulfilled by the lead contact Andrew Bolton ([andrewdbolton@gmail.com](mailto:andrewdbolton@gmail.com)).

#### Materials availability

This study did not generate new unique reagents.

#### Data and code availability

The data and code for analysis used in this study are publicly available as of the date of publication on Github including barrier locations, sizes, and raw escape trajectories for each trial performed by all fish. DOIs are listed in the key resources table.

### EXPERIMENTAL MODEL AND SUBJECT DETAILS

All wild-type experiments were performed on dpf 7–9 larval zebrafish of the WIK strain (ZFIN\_ZDB-GENO-010531-2, <https://zfin.org>). For the Mauthner ablation experiments, a transgenic fish generated by our laboratory (Tg(pMH93-16946)<sup>a378</sup>, <https://zebrafishexplorer.zib.de/home>) was crossed to a UAS-Kaede reporter line (Tg(UAS-E1b:Kaede)<sup>s1999t</sup>; ZDB-ALT-070314-1, <https://zfin.org>), yielding green fluorescence in both Mauthner neurons. Tg(pMH93-16946)<sup>a378</sup> was created via random Tol2 insertion of a plasmid described in Figure S4. All fish were fed daily with paramecia starting at dpf4. Experiments were conducted according to the guidelines of the National Institutes of Health and were approved by the Standing Committee on the Use of Animals in Research of Harvard University.

### METHOD DETAILS

#### Behavioral Setup

After a morning paramecia feeding, fish were added to a 12 cm-diameter acrylic tank with clear bottom and black walls. The tank was then mounted atop a clear acrylic stage. Fish behavior was recorded from above by a Mikrotron EoSens camera capturing at 500 Hz and 1280 x 1024 pixel resolution. Custom C# acquisition code was written for high-speed video writing, online background subtraction, stimulus delivery, and fish detection (available on Github). The entire rig was enclosed in black cardboard and tarp to minimize external light and noise, and all behavioral experiments were conducted in a dark room. A space heater was placed within the rig in order to maintain zebrafish at approximately 27° C. The tank was illuminated from below with an infrared light array to allow imaging in both light and dark conditions. Additionally, to draw fish into the center of the tank where barriers were located, a radial gradient phototaxis stimulus was projected onto a cold mirror and reflected onto the bottom of the tank, which was covered with a white diffusive screen. Once fish reached a threshold distance from the tank center, projector illumination was switched to bright whole-field light gray, which strongly lit the walls of the tank enclosure, reflecting light both onto the bottom and top of the tank. In dark trials, the projector was instead turned to whole-field black and automatically covered with a filter-flipper to block all light. Thus all escape

stimuli were delivered under bright whole-field gray illumination or darkness (except one condition described in [Figure 3](#)). For experiments with physical barriers, circular pieces of extruded acrylic were affixed to the bottom of the dish with inert dental wax. Unless explicitly described in the text as white, barriers were dark red in color. In virtual barrier experiments, circles the same width and color as the smallest physical barriers (12 mm diameter) were projected onto the floor of the tank. Throughout the entire trial, the acquisition program logged the XY coordinates of the fish, as well as the coordinates and dimensions of the barriers. If the fish came within the trial's threshold distance of a barrier edge, a stimulus command was sent via a PyBoard microcontroller to an electromagnet affixed to the stage. The electromagnet drives a metal rod into the stage for 200 ms, inducing a non-directional auditory startle stimulus (a "tap").<sup>23</sup> An LED light was fixed to the top of the metal rod such that its reflection into a mirror situated atop the stage was captured by the camera. From the LED reflection's movement across the mirror, the exact timing of the tap was extracted at 2-millisecond resolution (500Hz acquisition) by Python-based analysis code (available on Github). There were two metrics for excluding fish in our assay: fish were excluded from analysis if they failed to enter the barrier zone for 5 minutes, 5 times, before completing 5 escape trials (20.2% of total tested fish). Second, we excluded fish if the LED indicating stimulus delivery indicated that the stimulus was not evoked. Lastly, because we excluded the frontal-most visual field ([Figures 1](#) and [3](#)) from analysis between barrier conditions, we required that fish must have performed at least 3 trials in the given condition to be given PI or BAI score.

**Snell's Window:** For all solid barrier conditions, the top of the barrier protruded above the water surface. By calculating apparent height due to refraction and checking for the collapse of the image into the horizon of Snell's Window,<sup>48</sup> we confirm that the tops of all tested barriers are visible to the fish, and that distortion of the barriers at the distances tested is minimal (the image formed by a 4 mm distant barrier of 6 mm height occupies 97.5% of the retinal height subtended by the 8 mm distant barriers at 12 mm high). Water refractive index used in our calculations was 1.333 and depth of the fish eye underwater 1 mm.

## QUANTIFICATION AND STATISTICAL ANALYSIS

### Escape Analysis

Upon receiving a tap stimulus, all fish engaged in fast escape swims characterized by initial high angle turns and a subsequent burst of speed ([Figure S1](#)). To uncover the tail angle and direction of escape trajectories relative to barriers, 500Hz videos of escape sequences were background subtracted and dynamically thresholded using an OpenCV-based recursive contour-finding algorithm that terminated after finding a fish-sized object. We define angle of approach as the angle between the vector defined by the fish's longitudinal axis (a.k.a. its "heading vector") and a vector drawn from the fish's center of mass to the center of the approached barrier. If this value is negative we consider the barrier in the left hemifield with respect to the longitudinal axis of the fish, and vice versa for the right hemifield. The art in the paper that shows the barrier location with respect to the fish is a descriptor – if the barrier is on the left in figure art, it encompasses all trials where the barrier center was in the left hemifield (i.e.  $-25^\circ$  to  $-180^\circ$  angle of approach) and vice versa for barriers on the right in the figure art ( $25^\circ$  to  $180^\circ$ ).

To analyze escape direction, we used the calculated heading vector averaged over the 20 ms before tap stimulus command to rotate the XY coordinates of the escape trajectory (20ms - 60ms after tap command) so that escape coordinates are calculated with the fish initiated vertically and its origin at point (0, 0). In this way, positive X coordinates reflect escapes to the right and negative X coordinates reflect escapes to the left. We considered an escape to be "left" if the sum of escape X coordinates was negative and "right" if positive; we considered the escape an "avoidance" if the angle of approach to the barrier was opposite in sign to the X coordinate sum. If the fish collided with the barrier during its escape trajectory (determined when the center of mass is within 750 microns of the barrier edge), the direction of escape was calculated only up until the collision timepoint and a collision was registered. This prevented the assignment of "avoidance" to trajectories where fish deflect off of barriers.

For tail angle calculation ([Figure S1](#)), the tail was split into 6 segments and cumulative angles were calculated using dot products between segment vectors with direction determined by the cross product. The timeseries of tail angle sums was filtered with a Gaussian (standard deviation = 1 time div). Relative maxima and minima of tail angle sums were calculated and the largest tail angle (thresholded at  $50^\circ$ ) occurring within 100 ms of tap command was recorded. 97% of trials resulted in this type of large angle turn after tap delivery; the average latency from tap stimulus arrival to max tail angle is 11 ms and the average amplitude at max is  $104.4^\circ$ , which are nearly identical to escape turn recordings from other studies.<sup>23,24</sup> In our preparation, zebrafish are free to swim naturally and, because they must reach a certain location of the tank to receive a stimulus, can receive taps in the middle of a natural swim bout that has lead them near a barrier. Therefore, the baseline tail angle is quite noisy compared to other reports (e.g. Lacoste et al.<sup>23</sup>) where fish are embedded in agarose. Our characterization therefore determines latency as the time from stimulus delivery until absolute maximum tail amplitude is reached, not until the initiation of the escape as in these other reports.

### Navigation Assay

To record the fish's natural responses to obstacles while navigating, larvae that had never experienced taps in the vicinity of barriers were subject to the same experimental paradigm as above (e.g. phototaxis to attract the fish to the center, whole-field gray projection once barriers have been reached), except no taps were delivered when fish neared a barrier. The XY position of the fish and barriers, and the dimensions of the barriers, were tracked and plotted in [Figure 3](#); for heatmaps reflecting the fish's preferred swimming distance with respect to barriers, XY coordinates of the fish for every time point during navigation were calculated with respect to the nearest barrier. The coordinate system's origin is therefore set as the nearest barrier center over time. Visited pixel locations were binned by Gaussian filtering (standard deviation = 5) for the heatmap matrix representing the coordinate system.

### Mauthner Neuron Ablations

Phenylthiourea (PTU) treatment inhibits melanogenesis only over the duration of treatment so melanogenesis resumes on removal from the solution;<sup>49,50</sup> we used PTU on fish before laser ablation to avoid damage caused by laser heating of melanocytes. (Tg(pMH93-16946)<sup>a378</sup> x Tg(UAS-E1b:Kaede)s1999t)) embryos were collected into 100 M phenylthiourea (PTU) embryo water solution. Larvae were allowed to develop in PTU solution starting at around 18 hpf until they were removed for ablation at 4 dpf. Larvae were returned to filtered fish water post-ablation and allowed to recover for two days. In practice, we found that PTU treatment decreased pigment expression but did not fully abolish pigmentation. Pigmentation increased upon removal from solution; this was necessary for detection of the tail during escape behavior. PTU treated larvae were screened on 4 dpf for minimal pigmentation and Kaede expression in both Mauthner cells. Only Kaede positive larvae in which both Mauthner cells were visible were used for ablation. Larvae were then embedded in 1.8 % low melting point agarose in the center of a petri dish. Mauthner neurons were localized under two-photon excitation. Laser pulsing at 800-850nm at 360 mW for 1-.3 seconds was used in 5-10 locations on the Mauthner neuron. This induced Mauthner cell explosion in a subset of fish; gross morphological deformation was visible under 950 nm illumination after successful ablations, confirming that disappearance of the cell was not due to photobleaching. Any larvae where clear explosion of the Mauthner did not occur after multiple ablation attempts were discarded. Larvae were then freed from agarose and allowed to recover for two days. They were fed with paramecia on the first day post-ablation (6 dpf) and behaviorally assayed from 7-9 dpf as described above.

We note that in the optical section of the hindbrain area where we perform ablations, Tg(pMH93-16946)<sup>a378</sup> typically contain only two labeled neurons – the Mauthner pair. This was extremely beneficial for the specificity of our experiment,<sup>51</sup> but prevents performing clean control sham ablations because the 2P laser should theoretically prevent plasma generation in neurons that do not contain fluorophores at our chosen laser power. The unablated Mauthner cell adjacent to the ablation was inspected and completely intact in all preps, which served to control against local spread of the ablation. The escape bias in non-barrier conditions (Figures 4B and 4C) and the pattern of escape in ablated conditions (Figures 4C and 4D) suggests unilateral Mauthner ablation as the most likely interpretation.